INTERNATIONAL TABLES FOR CRYSTALLOGRAPHY

ISSN 1574-8707
it.iucr.org

Volume I, X-ray Absorption Spectroscopy and Related Techniques
ISBN: 978-1-119-43394-1

XAS cryostats and cryogenic studies

Olivier Mathon,[a]* Philippe Ohresser[b] and Ricardo Steinmann[a]‡

[a]ESRF, 71 Avenue des Martyrs, 38000 Grenoble, France, and [b]Synchrotron SOLEIL, L'Orme des Merisiers, 91192 Saint-Aubin, France. *Correspondence e-mail: mathon@esrf.fr

‡ Present address: AS Special Devices, 8 Avenue Victor Hugo, 38130 Echirolles, France.

Keywords: XAS; EXAFS; low temperature; cryostats.

This chapter describes cryostats dedicated to X-ray absorption spectroscopy (XAS) studies at cryogenic temperatures. The first section lists the reasons for exposing a sample to cryogenic temperature in an XAS study and the requirements in terms of temperature range and temperature stability. The second section is focused on the specific technical constraints linked to low-temperature XAS studies. The final section describes some of the main cryogenic technologies used at XAS facilities and discusses their respective advantages and disadvantages.

1. Why use cryogenics in XAS studies?

Varying the temperature, below or above room temperature, is one of the most important parameters when performing an experimental XAS study. Temperature is, on one hand, intimately entangled in the extended X-ray absorption fine-structure (EXAFS) equation through the dynamic part of the Debye–Waller factor. On the other hand, it is a key parameter of the chemical and physical properties of matter. As a consequence, there are two main reasons to subject a sample to cryogenic temperature. Firstly, it may be needed to improve the quality and the reliability of the XAS measurement by limiting thermal damping or slowing down X-ray beam-induced radiation damage. Secondly, it may be required to force the sample into a specific chemical/physical state. As a result, around one third of requested beamtime on an XAS beamline is devoted to low-temperature studies, often with temperature being a variable parameter. Cryostats are therefore key instruments at XAS facilities.

1.1. Thermal damping

The basic EXAFS equation (Chantler, 2021) can be approximated by

$$\chi(k) = \sum_j \frac{N_j S_0^2 F_j(k) \exp[-2R_j/\lambda_j(k)] \exp(-2k^2\sigma_j^2)}{kR_j^2} \times \sin[2kR_j + \Phi_j(k)], \quad (1)$$

where $\sigma^2 = \langle (r - \bar{r})^2 \rangle$ represents the mean-square relative displacement (MSRD) of neighbours with respect to the absorber due to static and thermal disorder (Sevillano *et al.*, 1979; Fornasini & Grisenti, 2015). Through the exponential factor $\exp(-2k^2\sigma^2)$, the temperature plays a fundamental role by damping the EXAFS oscillations, in particular at high k. It is of fundamental interest to use a cryostat to minimize this factor in an EXAFS study, thus increasing the amplitude of the EXAFS oscillations. Obviously, a visible effect can only be obtained when thermal disorder dominates with respect to static disorder (for example chemical disorder). From a

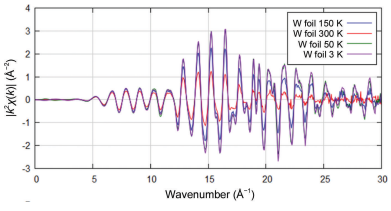

practical point of view, the temperature only needs to be decreased to values where thermal vibrations no longer dominate the damping at high k (Fig. 1). In many systems, this already occurs at 50–80 K. Therefore, a cryostat dedicated to minimizing thermal damping does not need to reach a low temperature nor to be precise in temperature determination and control. For example, a cryostat operating at nitrogen temperature is sufficient.

1.2. X-ray beam-induced radiation damage

Minimization of radiation damage is another important motivation for using a cryostat. Due to the flux increase and the reduction of focal spot size at third/fourth-generation synchrotrons, it is a fundamental and pertinent question. XAS is an element-specific technique and is primarily sensitive to local damage effects. Compared with diffraction, the problem is particularly critical in spectroscopic applications, where X-ray beam-induced damage is enhanced by the necessity to work around an absorption edge: for example, photo-reduction has been observed to occur between one and two orders of magnitude below the Henderson limit (Schooneveld & DeBeer, 2015). An X-ray flux of up to 10^{13} photons s^{-1} focused in a 10 × 10 µm spot is nowadays common. At 7 keV, it delivers a power of the order of 11 mW, which corresponds to a power density of up to 100 MW m^{-2}. A useful indicator is the skin dose, which corresponds to the dose deposited in the mass of a volume defined by the X-ray spot size and the attenuation length. This skin dose is in general higher at low energy (<2 keV) due to the small penetration depth. Starting from our previous example, the skin dose over 1 s at the Fe K edge (2950 MGy at the edge + 50 eV) is 4.7 times smaller than at the Fe L_3 edge (edge + 50 eV). In addition to the heat load delivered directly to the sample and the resulting problem for efficient cooling and temperature determination, the intense X-ray beam induces various phenomena such as photo-reduction, photo-oxidation, breakage of bonds *etc*. All of these effects deeply modify the fundamental state of the sample and consequently the XAS spectrum. These phenomena have been reported, for example, in XAS studies in chemistry (Mesu *et al.*, 2006), environmental sciences (Manceau *et al.*, 2002; Wang *et al.*, 2019) and biology (George *et al.*, 2012). Obviously, when possible, the best solution to minimize beam damage is to reduce the photon dose delivered to the sample by decreasing the flux (attenuation) or the flux density (defocusing). A well established method to slow down or even prevent the radiation-damage process is to decrease the sample temperature (Latimer *et al.*, 2005; George *et al.*, 2012; Wallander & Wallentin, 2017). In general, when such a method is effective, the lower the temperature, the lower the radiation damage. Therefore, cryostats used for this purpose need to reach low temperature (below 10 K) but do not need to be precise in temperature determination and control (<2 K). However, the use of a low temperature below 10 K to prevent photo-induced chemistry has to be envisaged carefully when the sample is subject to subtle chemical and structural changes with temperature.

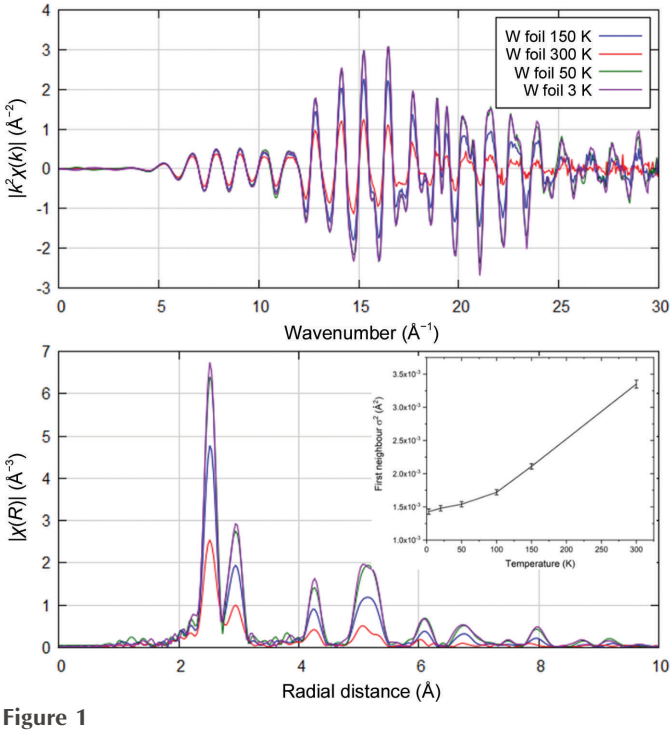

Figure 1
Effect of temperature on the damping of EXAFS oscillations recorded on a tungsten foil at the W K edge at four different temperatures (300, 150, 50 and 3 K). Top: $k^2\chi(k)$; oscillations at high k are more damped. Bottom: magnitude of the Fourier transform; all scattering paths are strongly affected. The inset represents the value of the Debye–Waller factor (σ^2) fitted for the first W–W shell as a function of temperature; below 70 K the σ^2 variations become negligible.

1.3. Temperature-dependent and phase-transition studies

X-ray absorption near-edge structure (XANES) spectroscopy is sensitive to the electronic structure, while EXAFS gives access to local structural parameters. Therefore, it is natural to couple cryostats to XAS to study temperature-dependent and phase-transition phenomena. A temperature-dependent XAS data set allows the extraction of chemical and physical properties of matter such as thermal expansion (Cao *et al.*, 2003; Abd el All *et al.*, 2012; Fornasini & Grisenti, 2014; Bridges *et al.*, 2014; Fig. 2), bond stiffness (Yamazoe *et al.*, 2016) and lattice dynamics (Timoshenko *et al.*, 2014) and thermodynamic parameters such as Debye or Einstein temperatures (Dalba *et al.*, 1995; Mizumaki *et al.*, 2011). Observation of the evolution of the MSRD as a function of temperature may yield an estimation of static and dynamic MSRD contributions (see, for example, Caramazza *et al.*, 2016). It is also worth noting that simultaneous fitting of a temperature-dependent XAS data set may help to decrease the number of free parameters and thus reduce the error bars. Temperature studies can be used to disentangle the interplay of metallic and molecular behaviour of gold nanoclusters (MacDonald *et al.*, 2011). Various phase transitions at defined temperature can be studied, such as the famous Vervey transition in Fe_3O_4 (Subías *et al.*, 2005) or metal-to-insulator transitions (Croft *et al.*, 2003). Low-temperature XAS studies

are particularly suitable for the study of phenomena related to magnetic properties, such as heavy fermions (Okane *et al.*, 2012), spin-crossover transition (Okabayashi *et al.*, 2015) and superconductivity (Joseph *et al.*, 2010).

In these cases, the temperature needs to be perfectly stabilized, controlled and measured with a precision better than 0.1 K. The accessible temperature range should be as large as possible (2–300 K), even to values significantly higher than room temperature (∼1500 K), where ovens are required. In the latter case, cryostats covering the temperature range from 2 to 450/500 K are particularly suitable as they allow experimental overlap with measurements performed using high-temperature ovens.

1.4. Ultralow temperatures below 1 K

The wide range of cases requesting low temperature includes particular applications that need an ultra-low temperature (ULT) in the subkelvin range or even well below 100 mK. ULT is key when dealing with new states of matter and quantum phenomena. However, the environment of an XAS setup is constrained in terms of the lowest achievable temperatures (see Section 2.5), limiting research to systems where several hundred millikelvins are sufficient to address the scientific question. This includes, in particular, studies of magnetic phenomena, such as spin transitions, magnetic ordering, relaxation of metastable states, superconductivity, the Kondo effect *etc*. When the thermal energy is smaller than the energy difference between the ground-state and the first excited levels, the ground-state properties can be revealed, which is of primary interest for a spectroscopic technique such as XAS.

In this range of application, molecular magnetism has seen a breakthrough thanks to the coupling of XAS and dichroism measurements in X-ray magnetic circular dichroism (XMCD) and X-ray natural linear dichroism (XNLD). One of the most interesting magnetic properties, first observed with Mn_{12}, is quantum-tunnelling magnetization, which is characterized by evenly spaced steps in the hysteresis curve (Gatteschi & Sessoli, 2003). Such a property means that one molecule can be in several well defined quantum states and therefore may potentially be a building block for a quantum computer. However, in order to exploit such promising behaviour in a device, it is mandatory to form ordered single-molecular films on a surface. The process of the deposition of such molecules on a substrate is likely to modify their properties. The high sensitivity of XAS and XMCD can be used to monitor the electronic and magnetic properties of supported single-molecular films. The quantum nature of the phenomena makes the use of ultralow temperature mandatory. The first successful observation of quantum magnetization on a self-assembled monolayer of Fe_4 was obtained by XMCD performed at 500 mK (Mannini *et al.*, 2009). Several other studies have completed the picture and the use of a new dilution insert combined with improved thermal shielding has allowed the lowest temperature to be decreased to 220 mK (Kappler *et al.*, 2018).

2. Constraints of XAS studies at low temperature

An XAS experiment presents a certain number of characteristics that influence the technical aspects of a cryostat. It is not realistic to think that a single cryostat can manage all kinds of experimental situations, but basic rules can be retrieved from

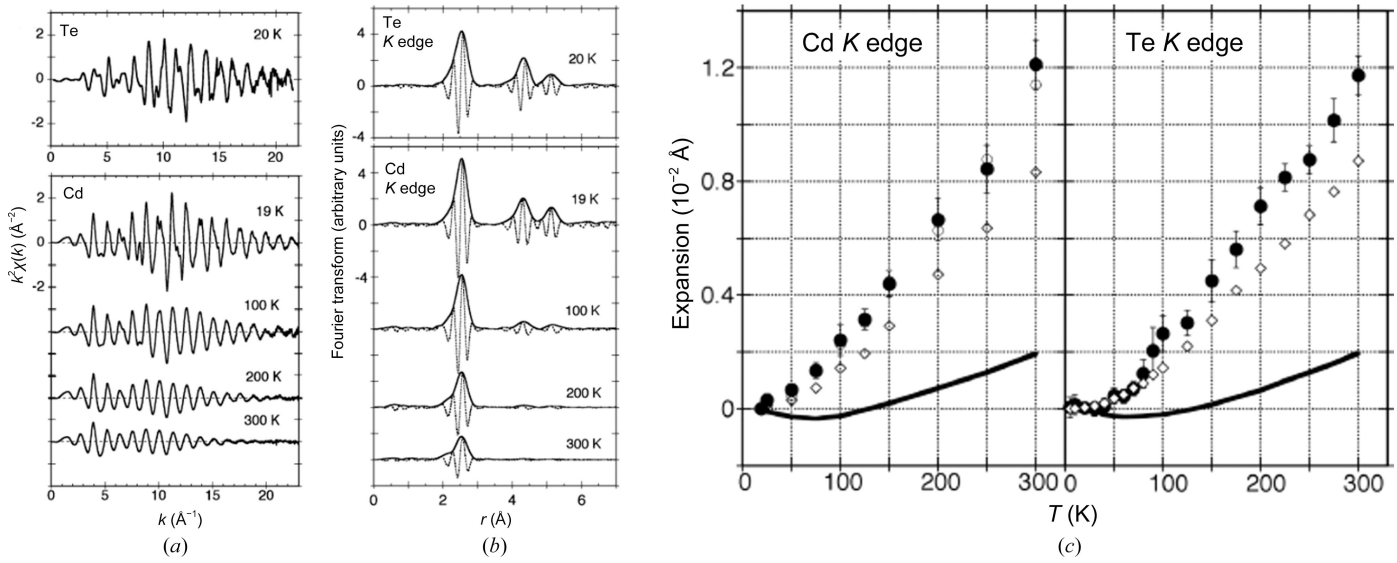

Figure 2
EXAFS study of negative thermal expansion in CdTe crystals from Abd el All *et al.* (2012). (*a*) Cd and Te *K*-edge $k^2\chi(k)$ EXAFS signals as a function of temperature. (*b*) Modulus and imaginary parts of the corresponding Fourier transforms. (*c*) Thermal expansion of the first-shell distance from cadmium and tellurium EXAFS. Full circles: relative values δC_1^* from the ratio method (with error bars). Diamonds: contributions of the distribution asymmetry to the thermal expansion (from third cumulant). Open circles: relative values from *IFEFFIT*. Continuous line: apparent bond expansion δR_c derived from the lattice thermal expansion. The combined analysis of the temperature data sets at both the Cd and Te *K* edges allows experimental disentanglement of the bond-stretching and tension effects with resolution better than 0.001 Å and a closer insight into the negative thermal expansion properties.

XAS setup characteristics to optimize the cryostat choice/design. In the following paragraphs, we review the technical aspects that are mandatory to combine low temperatures and XAS.

2.1. X-ray beam access and X-ray beam detection

XAS measurements are performed, by definition, using X-rays close in energy to an absorption edge. Nowadays, XAS beamlines constructed at third- or fourth-generation synchrotrons are able to deliver 10^{13} photons s^{-1} on the sample. The X-ray beam is a source of power that is directly dissipated into the sample. The thermal load of the X-ray beam is difficult to estimate, as it depends on the absorption and the de-excitation processes in the sample. Nevertheless, one can at least estimate the maximum power (W) carried by the X-ray beam as W (J) = flux (photons s^{-1}) × energy (eV) × 1.602×10^{-19}. At 7 keV a beam of 10^{13} photons s^{-1} provides a thermal load of 11 mW, while at 1 keV a beam of 10^{12} photons s^{-1} leads to a maximum power of 160 µW. An intense X-ray beam does not only induce radiation damage but also affects the lowest temperature accessible by a cryostat. Moreover, it prevents precise determination of the sample temperature in the measurement area, since values will be highly dependent on the thermal diffusivity of the sample, as discussed in Section 2.5.

X-rays need, at a minimum, to enter the cryostat and the absorption process needs to be detected. A major source of thermal perturbation is the need to open windows in the cryostat for X-ray beam access and X-ray beam detection: at least one window for the incident X-ray beam in total electron-yield (TEY) mode and a second window in transmission and fluorescence mode. Often three windows are necessary to switch between different detection modes. Moreover, in many cases additional optical accesses are required for sample transfer or other purposes such as sample excitation (with a laser for example). The radiated power P per m^2 related to the thermal load can be estimated to a first approximation with the Stefan–Boltzman law $P = \sigma \times \varepsilon \times T^4$ (where $\sigma = 5.67 \times 10^{-8}$ W m^{-2} K^{-4} and ε is the emissivity of the black body). For instance, an access port of ∼4 cm in diameter (12.5 cm^2) at 300 K will radiate 600 mW. Each window or surface above the working temperature represents a source of heat load that radiates into the measurement chamber. It is important to minimize the number and the size of such windows and surfaces and to shield them thermally when possible. At low energies, typically below 4 keV, a special design must be developed to limit the absorption of X-rays by windows. For example, a high-purity unsupported aluminium foil (thickness = 0.7 µm), used as a thermal screen on the entrance window, reduces the incoming flux at the Fe $L_{2,3}$ edge energy by a factor of two.

To limit the number of windows, the detector can be incorporated into the measurement chamber (McFarlan Holman *et al.*, 2004). This has the additional advantage of increasing the detection solid angle by reducing the distance between the detector and the sample. At the same time, any detector will radiate a non-negligible thermal load. This effect has to be carefully considered, in particular when anticipating subkelvin temperatures on the sample. In the case of diodes, the simplest way is to mount them on a support cooled at 4 K. In the case of TEY, one has to deal with the fact that the sample needs to be electrically insulated, while excellent thermal conduction is simultaneously required to reach low temperature on the sample. This can be obtained by using a sapphire ring ($R > 200$ GΩ) to electrically decouple the sample from the sample holder.

2.2. Constraints linked to the sample

The first constraint is the diversity of the samples to be measured. Samples can be solids, liquids or gases; they can be single crystals, polycrystalline powders, laminated foils, glasses, thin layers deposited on substrates or pressed powder pellets; they can have different sizes and shapes; they can be hazardous materials or fragile samples that should not be contaminated by any material present in the cryostat. An initial answer to this diversity is to develop a set of sample holders dedicated to each case: liquid cells, pellet cells, multiple-sample holders, isolated cells for hazardous/fragile sample and so on.

The sample can be a metal, a semiconductor or an insulator, and thus its thermal conductivity can vary greatly. For efficient thermal cooling, better homogeneity of the temperature in the measurement area and consequently better precision in determination of the sample temperature, it is recommended to use an indirect, rather than a direct, cooling scheme. In the direct cooling scheme, the sample is fixed on the cold plate and the transmission is dependent on the thermal diffusivity of the sample, the sample-holder material and the mechanical/thermal quality of the interfaces. In the indirect cooling scheme, the sample is homogeneously surrounded by a contact gas (generally helium) thermalized by the cold plate. However, in many situations, when the experiment is under vacuum or at a very low temperature where the exchange gas could be liquefied, the indirect cooling scheme is not possible.

2.3. Operation at low energy: UHV constraints

Among the variety of XAS setups optimized for different sample environments, there is the particular case of ultrahigh-vacuum (UHV) experimental stations. UHV is often used on low-energy beamlines (typically below 2000 eV). Indeed, the use of photons below ∼2 keV has two consequences: a low penetration depth of the X-rays and poor efficiency of the fluorescence yield in favour of the electron yield. Vacuum is required to avoid the strong absorption of soft X-rays and is most often mandatory when using TEY. The escape depth of the electron is typically around tens of nanometres, meaning that the measured signal comes from the surface and UHV is necessary to prevent surface contamination. To attain UHV conditions, apart from the adapted pumping, one has to use UHV-compatible materials, which can be constraining when choosing a technical solution for a cryostat. UHV conditions drastically limit the versatility of such a cryostat. Samples are

directly mounted on the cold plate of the cryostat using a manipulator. No solution using an exchange gas can be used to cool the sample.

2.4. Materials

Materials and their intrinsic properties for cryogenic applications (body parts, seals, windows, thermometers *etc.*) are not specific to XAS applications and are beyond the scope of this article. Further details of this can be found in textbooks (Conte, 1970; Pobell, 2007; Richardson & Smith, 1988). However, some specific properties of materials that are directly related to XAS experiments are discussed below.

When performing XAS measurements, due to diffuse beams special attention must be paid when the edge energies of the studied elements in the sample are close to those of the elements present in the cryostat components. This is particularly true when performing measurements on a dilute sample at any edge of the 3*d* elements. Copper, iron, nickel, chromium and manganese are major alloy components used in cryogenic technologies. Precaution can be taken in the choice of the sample-holder material; PEEK polymer may be preferred over aluminium or copper-based materials at the expense of thermal conductivity. Copper and aluminium alloys are also widely used, in particular for the measurement chamber. Cryostat design can incorporate shielding of the measurement chamber with ultrapure aluminium foil to minimize fluorescence pollution at the 3*d* metal *K* edge. In any case, when performing an experiment on a dilute sample with absorber concentrations below 100 p.p.m. the measurement procedure should include a blank XAS measurement to evaluate spurious contributions from the cryostat itself.

As already mentioned, windows are key elements of a cryostat. Windows for XAS must be mechanically compatible and leak-tight (with vacuum insulation of the measurement chamber, for example). Windows must be well adapted to low temperatures. When placed in the X-ray beam path, windows must (i) be as transparent as possible to the X-ray beam, (ii) not contain elements with edges within the energy range of interest and (iii) be resistant to X-ray beam radiation damage. Above 4 keV, Kapton polyimide film is often used for cryostat windows; Mylar (PET) can also be used when visible optical access is needed, although Mylar is more sensitive to radiation damage. At low energy, windows are mainly used as thermal shielding to limit parasitic infrared (IR) radiation. In addition to the conditions previously, the shielding window must be a good thermal conductor and be thermalized. Thin (<1 µm) unsupported aluminium films are used for such purposes. For visible optical access, sapphire windows or a semi-transparent heat absorber can also be used to shield the incoming IR radiation.

2.5. Temperature range, effective temperature and temperature calibration

The lowest temperature accessible in a cryostat is defined by the cryostat technology (see Section 3) and by the balance between the cooling power and the heat input.

As previously mentioned, the heat is transferred by thermal conduction through the cryostat structure or any other elements linked to room temperature such as thermometers and heater wires, as well as by radiation through the windows and by the power loaded by the X-ray beam. For a sample thermally well anchored on the cold plate and a cryostat with a cooling power of 30 mW at 2 K, the lowest temperature accessible depends, on one hand, on the incoming IR radiated through the windows and, on the other hand, on the X-ray beam power. For instance, in our experience, the heat irradiated by a window at room temperature will increase the lowest working temperature by about 0.3 K cm^{-2}. In this range of temperature and heat power, a cryostat with a base temperature of 2 K equipped with a 1 cm^2 window will operate at 2.3 K if the X-ray beam power absorbed by the sample is negligible. The temperature measured on the cold plate will be close to the sample temperature. As the cooling power increases with temperature, heat input has a less dramatic effect at higher temperature. The effect is not linear: for a cryostat equipped with two windows for transmission and a third window compatible with a multi-element fluorescence detector (diameter 60 mm), the total area of the windows is about 30 cm^2; the lowest temperature reached by such a cryostat will be close to 5 K on the cold plate.

The situation is different when the X-ray beam power cannot be neglected. This is the case when the power density is 'too high' for thermal diffusion of the sample, for the thermal resistance between the sample and the cold plate or for the cooling power of the cryostat. As already mentioned, 10^{13} photons s^{-1} at 7 keV represents a local heat load of 11 mW. When focused on 100 µm^2, it is equivalent to a power density of 100 MW m^{-2}. The effective temperature, *i.e.* the temperature of the sample under X-ray beam irradiation, will be remarkably different from the cold-plate temperature provided by the thermometer. It will also generate a temperature gradient between the centre and the border of the sample. If a 1 mm diameter disk of pure gold, with a thickness of 0.1 mm and a thermal diffusivity of 1.3 × 10^{-4} m^2 s^{-1}, is mounted in a cryostat with a base temperature of 2 K on the cold plate, the temperature at the X-ray beam impact can be as high as 4.6 K and will be close to 2.7 K at the border of the disk. The thermometer on the cold plate will not be sensitive to the increase in the sample temperature. The sample will never be in equilibrium with the cold plate and the thermometer will measure ∼2.3 K. If the sample is a porcelain ceramic disk (thermal diffusivity of 0.4 × 10^{-6} m^2 s^{-1}), the temperature would reach 530 K at the centre and 134 K on the border in the same cryostat! These values are derived from simple models using rough approximations, but point to a possible large discrepancy between the temperature sensor and the effective temperature of the sample at the X-ray beam position. Robust calculations using finite-element methods can be used to estimate the temperature of the sample under X-ray beam illumination (Wallander & Wallentin, 2017). In extreme cases, the real temperature of the sample could be difficult to estimate as it depends on intrinsic sample properties such as absorption (which will vary through the absorption

edge), thermal conductivity, geometry and extrinsic factors such as thermal contact (heat-transfer coefficient) with the cooling plate, and beam characteristics. Another consequence of such a discrepancy between the effective temperature and the thermometer temperature is the presence of a large temperature gradient in the sample volume under X-ray irradiation. As XAS is an 'average' technique over all absorber atoms, a large temperature gradient will result in a sum of different thermal states. Beam inhomogeneity will probably lead to the same kind of result. When possible, reduction of the flux is the only way to measure a sample properly at low temperature.

Under intense X-ray beam illumination, calibration of the effective temperature versus the thermometer temperature is a challenge. Firstly, the thermometer has to be (i) as close as possible to the measurement area, (ii) well calibrated (ideally cross-calibrated with a probe fixed at the sample place), and (iii) well thermalized with the sample. If the temperature probe is far from the sample, and/or close to the heater or to the cold part, a strong shift between the actual sample temperature and the thermometer temperature will be observed.

A way to properly calibrate the thermometer is to measure a well known critical phenomenon on the sample of interest using XAS as a function of X-ray beam flux. For example, in Strohm *et al.* (2019), before starting the experiment, the authors measured the well known compensation temperature T_{comp} = 78.8 K between the two ferrimagnetic phases in $Er_3Fe_5O_{12}$ garnet as a function of flux. The authors reduced the flux up to the moment where the effective temperature and the thermometer temperature corresponded to the published data. In most cases such a direct approach is not possible and the link between the thermal probe and the effective temperature has to be established using different samples. For instance, measurements with an XMCD paramagnetic sample, the magnetic signal of which strictly depends on the temperature, will provide a good measurement of the effective temperature under the beam and will allow calibration of the thermometer (Kappler *et al.*, 2018). As an ultimate test on an unknown sample, a second measurement with reduced flux allows evaluation of whether the effective temperature may differ from the thermometer temperature.

2.6. Practical aspects

Some practical aspects need to be considered when combining a cryostat with an XAS experiment. In general, the XAS beamline staff and the beamline users are not cryogenic specialists; the cryostat should be robust, easy to install and easy to operate. Modern XAS beamlines are generally versatile and can hold many different sample environments, so the implementation and the standby of the cryostat on the beamline should be (when possible) as short as possible (∼2 h) and the first cooling cycle should not exceed one hour.

To facilitate user operation the cryostat should ideally be equipped with a sample-transfer chamber (or airlock chamber). These models are referred to as 'top-loading cryostats'. The airlock chamber allows the sample to be changed while keeping the cryostat at low temperature, thus avoiding a costly and time-consuming operation. In a top-loading cryostat, sample change and cooling to operation temperature requires less than 15 min.

The cryostat must be equipped with a set of sample holders that enable it to cope with diverse sizes and structures (pellets, foils, small samples *etc.*), states (solid, powder, liquid) and detection configurations (transmission, fluorescence, TEY). If the cryostat is equipped with a sample-transfer rod, the possibility of holding more than one sample on the sample holder (fixed at the bottom of the rod) leads to more efficient use of beamtime. The cryostat can include mechanical vertical and horizontal translations to align the sample with respect to the X-ray beam (see Fig. 3). The translations also allow the position of the sample to be adjusted to compensate for thermal expansion when the temperature is modified. The sample may be mounted on a rotation stage in order to switch between different detection modes (transmission or fluorescence) and for polarization and/or angular-dependent studies.

An important practical parameter of a cryostat is the liquid helium (L-He) consumption. Changing the L-He dewar or refilling the L-He container during a running experiment is a delicate operation. The risk of blocking the cryogenic circuit, with inherent loss of beamtime, is high. A dewar with a 100 l capacity should be sufficient for a full week of operation at the lowest temperature; this corresponds to a L-He consumption of about 0.5 l h^{-1}.

Another aspect of the friendliness of a cryostat is the control of the temperature. In the case of a cryostat that allows a wide range of temperatures, an automaton that is able to control a whole set of parameters (heaters, valves, PID, sample

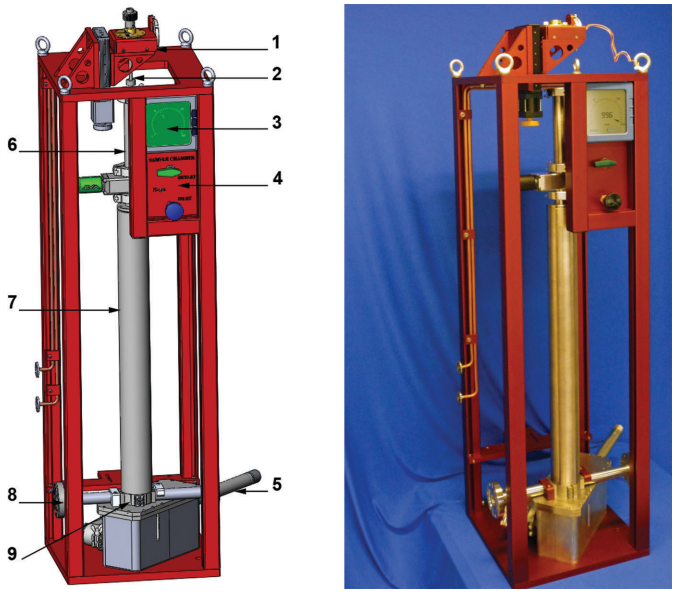

Figure 3
Example of a TL-CFC cryostat developed specially for XAS measurements. (1) Sample rotation for polarization-dependent studies, (2) sample vertical translation, (3) measurement chamber manometer, (4) vacuum/exchange-gas control (5), L-He cryogen input, (6) airlock chamber, (7) vacuum chamber, (8) transmission windows and (9) fluorescence window.

Table 1
Typical figures of merit for the principal types of cryostat used in XAS cryogenic studies.

Cryostat	Lowest T (K)	Cooling power	Sample change	Expense†	Advantages	Inconveniences
Closed cycle	4.5	100 mW at 4.5 K	3 h	50 000	Plug-and-play and reliable, does not need cryogen refill	Vibrations, low cooling power at low T
Bath cryostat	1.3	5 W at 4 K	30 min	30 000	Low base temperature, high cooling power, vibration-free	Needs regular refilling, large size and weight, complicated to operate, large standby
Continuous flow	2	1 W at 4 K	15 min	20 000	Plug-and-play and reliable, allows various geometries and sample environments, high cooling power, low He consumption, vibration-free	Remains attached to an external L-He dewar; external L-He dewar change during operation is a delicate operation
Dilution	0.2‡	150 μW at 100 mK	5 h	150 000	Can reach temperatures well below 1 K	Low cooling power, operation restricted to specialists, must remain mounted on the beamline, long standby time

† Running costs are not included. ‡ Under X-ray beam.

position *etc.*) is useful. It is possible to find a commercial product where the user only needs to define the set point. The automaton performs the entire control, even for complicated system such as dilution refrigerators.

Maintenance of the cryostat should be as simple as possible. For example, the X-ray windows can be damaged either by the X-ray beam or by a manipulation error. The windows should be accessible and easy to change (when possible, the windows should be clamped and not glued). This maintenance aspect is even more important for a cryostat working at UHV. As the cryostat needs to be baked out before operation, any intervention will be time-consuming.

3. Overview of cryostat technology for XAS applications

Several types of cryostats are available, with respective advantages and disadvantages. In this section, we address a selection of the most adapted cryostat technologies for XAS measurements. A comprehensive review of cryostat technologies and experimental techniques can be found in dedicated literature (Conte, 1970; Pobell, 2007; Richardson & Smith, 1988). Typical figures of merit for the principal types of cryostats used in XAS cryogenic studies are given in Table 1.

3.1. Gas blowers

Gas blowers are often used to refrigerate a sample for XAS measurements. In these systems a helium or nitrogen laminar gas stream with a controlled temperature is openly flowed directly over the sample. The principal advantages of this technology are its easy implementation, lack of infrastructure cost and the ability to work over a large temperature range between 80 K (4.5 K using L-He) and 500 K (van der Linden *et al.*, 2013). However, inserting the sample inside the flow transforms the laminar flow into a turbulent flow, leading to deposition of water or ice on the sample, which is detrimental to XAS normalization. This technology, which has widely been adopted in protein crystallography, is not recommended for XAS studies, where samples are larger and the measurement timescale is longer. In addition, as the cryogen is vented into the room atmosphere, the experimental area must be well ventilated, particularly when the device blows helium (with a risk of suffocation or embolism).

3.2. Closed-cycle coolers

A closed-cycle cryostat is a device that uses an external mechanical cooler based on a compressor to produce the cooling power; for example, a cylinder in which a piston (or a pulse tube) produces an isentropic expansion of helium gas that cools a copper plate (cold head) thermally connected to a sample chamber. These systems do not require a cryogen (hence the common name 'cryo-free') and thus do not need large infrastructure to be operated; however, the initial cost is high. In general, they are easy to operate and reliable but are delicate to mount. A temperature range between 4.5 and 300 K can be obtained with a single-stage device. Multi-stage devices are used to reach lower temperatures down to 1.5 K. The main drawback of these systems is the low cooling power that is available and consequently the long standby of several hours. The samples are in general directly mounted on the cold head. Warming to room temperature is necessary to change the sample. Mechanical vibrations can be also an issue depending on the model.

3.3. Bath cryostats

In these cryostats, the cryogen is stored in an internal container. In addition to the L-He, screening by liquid nitrogen is often needed. In its historic form, the cold plate (also named a cold finger in this case) of a bath cryostat is in direct thermal contact with the L-He. The sample, mounted on the cold plate, is cooled to 4.2 K. Nowadays, bath cryostats are equipped with a '1 K pot', an evaporation vessel of a few cm^3 filled with L-He from the internal container through a capillary. The evaporation vessel is pumped and the liquid from the main bath is isenthalpically expanded (a lowering of the vapour pressure), which consequently results in lowering the temperature (Pobell, 2007). The presence of the internal container and the large dimensions and weight (10–30 kg) make such cryostats more difficult to implement and to align. Tilts are limited to only a few degrees. These cryostats are complicated to set up and require a good knowledge of cryogenics for operation and adjustment. Stand-by to start the experiment exceeds one day and several days are required

to warm the system up. The real advantage is the base temperature, which can drop to the very low temperature of 1.3 K. Bath cryostats are generally permanently installed and may be used in combination with large setups such as, for example, superconducting magnets and/or ^{3}He/^{4}He dilution refrigerators.

3.4. Continuous-flow cryostat

The operating principle of these cryostats is to cool down the sample chamber by a cooling circuit in which the cryogenic fluid is stored in an external container (a storage dewar). The cooling principle of a continuous-flow cryostat is similar to the '1 K pot' process described above, except that the L-He is continuously and directly pumped from the dewar through the transfer line. The liquid flow is vaporized and passed through the main heat exchanger (cold plate). Helium gas is driven through a secondary heat exchanger, where part of the remaining gas enthalpy is used to cool thermal screens. Reaching temperatures from 2 to 500 K, this instrument can easily be adapted to variable beamline geometries and works in any orientation. Its mechanical modularity, high cooling rate and excellent temperature stability allows a wide spectrum of experiments. This type of cryostat presents numerous advantages: (i) it can cool down all varieties of samples regardless of their nature, size or form, (ii) several samples (mounted on the same sample holder) can be measured sequentially, (iii) sample change, including a complete temperature cycle, takes only a few minutes and (iv) it is a vibration-free instrument. The helium consumption is low (12.8 l per day at 2.5 K); a 100 l external dewar allows a one week of operation.

The sample can be directly anchored on the cold plate (often used at low energy; Kummer *et al.*, 2016) or driven into the measurement chamber by a top-loading device (often used at high energy). In the latter case, the most versatile solution for daily use is the top-loading continuous-flow cryostat (TL-CFC; see Fig. 3). In the measurement chamber, the samples are surrounded by a low-pressure helium contact gas (typically between 2 and 20 mbar) and are indirectly thermalized by the cold plate. The sample-holder rod can easily be positioned in front of the windows through a longitudinal and/or angular displacement table. Samples can be changed through an airlock chamber without having to heat the cryostat. To limit the contact-gas convection between room temperature and the cold plate and to restrict the entrance of heat by radiation, the sample-holder rod is equipped with thermal baffles. Temperature measurements can be performed precisely if the sample holder is fitted out with a thermometer. Nevertheless, for large samples (>10 mm) stratification of the exchange-gas column will produce a temperature gradient with a significant effect on the measurement. This effect is more prominent below 4 K. To give an order of magnitude, in a vertical measurement chamber of 25 mm diameter with a cold plate at 2 K, the temperature gradient is $\sim$0.08 K mm^{-1}. Beyond 10 K, the gradient is smaller and often within the error of temperature measurement.

An interesting evolution of the TL-CFC is the recently developed 'hybrid' cryostat, which combines temperature-controlled helium flow with a static column of gas. The main advantage of this device is that the sample is directly cooled by the helium flow. Among the many qualities of this cryostat are (i) the absence of stratification, (ii) a lower temperature limit and (iii) a particularly high accuracy in measurement of the sample temperature.

3.5. Dilution refrigerator

Measurements at subkelvin temperatures require the application of other cooling techniques. A liquid ^{4}He bath at ambient pressure allows temperatures down to 4.2 K to be reached. Pumping this ^{4}He bath can decrease the temperature to 1.3 K at 0.1 mbar. This limit decreases to 0.3 K when using a ^{3}He bath. However, the limited capacity of the ^{3}He pot confers autonomy for no longer than a few hours. To reach ULT in a persistent mode, one has to change both the coolant and the technology. A complete overview of millikelvin technologies can be found in Betts (1989). Currently, the most common subkelvin temperature refrigerators use either adiabatic magnetization of a paramagnetic salt or the particular properties of a ^{3}He–^{4}He mixture in the case of the dilution refrigerator. The principle of adiabatic magnetization forbids its use in magnetization studies and explains why dilution refrigerator systems are quite widespread at XAS beamlines. Temperatures as low as 2 mK can be achieved using dilution refrigerators, but the constraints of an XAS setup will not allow experiments to be conducted at such low temperatures (see Section 2.5).

The theoretical principles of dilution systems are described in detail in Pobell (2007) and Lounasmaa (1974). Dilution refrigerators use the particular properties of the phase diagram of a ^{3}He–^{4}He mixture: below 0.97 K this mixture undergoes phase separation between a dilute phase and a concentrated phase that are poor and rich in ^{3}He, respectively. Moreover, the concentration of ^{3}He in the dilute phase cannot be less than 6.4% even at $T = 0$ K. In a dilution refrigerator, the ^{3}He isotope is the main actor in the cooling process. It is cycled between three main stages (see Fig. 4): from 300 K (pumping stage) to the lowest temperature (mixing chamber) through a still at 1 K. A 4 K pot ensures initial cooling, which is traditionally obtained using liquid helium, but cryo-free cryostats are becoming more and more common, forming the so-called dry-dilution family. Further cooling is obtained by several heat-exchange and adiabatic relaxation process until the temperature allows phase separation in the mixing chamber. Gravity pulls the heavier fluid (the dilute phase) to the bottom, while the lighter fluid (the concentrated phase) floats on top. The still is connected to the dilute phase and pumping the still favours evaporation of the lightest isotope (^{3}He). Therefore, pumping actually induces depletion of ^{3}He in the dilute phase and consequently ^{3}He from the concentrated (rich) phase is transferred to the dilute (poor) phase to keep the concentration of ^{3}He in the dilute phase above 6.4%. This transfer and the different enthalpies of the two phases

constitute the mechanism that allows ULT to be reached in the mixing chamber.

In this temperature range, the cooling power is of the order of tenths of a microwatt. The heat loads due to IR radiation and X-rays have to be significantly lower to maintain ULT. The heating power of the X-ray beam needs to be perfectly monitored and the effective temperature must be determined with precision. Kappler *et al.* (2018) used two well calibrated samples: a paramagnetic $Er_{0.025}Pd_{0.975}$ alloy and an Fe_4 single-molecule magnet chemisorbed as a monolayer on Au(111). With these two reference samples, the authors confirmed that at around 200–500 mK the effective temperature under the X-ray beam was a maximum of 50 mK above the thermometer temperature. Due to the complexity of such an instrument, operation is usually restricted to researchers with extensive experience in cryogenics (Letard *et al.*, 2007; Palmer *et al.*, 2015; Beeck *et al.*, 2016). Nevertheless, dilution refrigerators with full and automatic temperature control are now commercially available.

3.6. Special cryostats

There are as many possible cryostats as there are XAS applications. XAS techniques are used in different environments and often require the development of special devices. A few examples are described below.

3.6.1. High-pressure cryostat. The investigation of matter under extreme conditions is one of most important research directions to improve our fundamental understanding of materials. XAS/XMCD techniques are increasingly being applied to probe the local structure, electronic and magnetic properties of materials subjected to high pressure or high magnetic fields *in situ*. Low temperature combined with high pressure and high magnetic fields involves the design of an instrument in which the mechanical stability, vibration level and thermal homogeneity are more delicate and complex than in a conventional cryostat. A sketch and a picture of a recently developed cryostat are shown in Fig. 5. The operating principle of the cryostat is that of any continuous-flow cryostat: helium (blue arrows) from a container is directly injected into the main heat exchanger (2) by means of a transfer line and cools the high-pressure cell (1). It passes through the secondary heat exchanger (3), where a large amount of the remaining enthalpy is used to cool the thermal screen (4) and reduce the radiation heat from the vacuum chamber (5). Finally, the gas is drawn through a coaxial transfer tube by a vacuum pump. The cryostat has a KF25 vacuum port (8) and its working pressure is typically about 10^{-7} mbar. To each heat exchanger, several heaters and a calibrated thermometer are fixed (7). Two symmetric telescopic supports (6) ensure compensation for the thermal expansion of the central tube, keeping the positioning of the measurement plane. Leak-tight connectors (9) draw out all electrical signals and a high-pressure fitting on the upper flange fastens the capillary to pressurize the diamond anvil cell. The cryostat is able to reach low temperatures of down to 4.6 K on the sample together with high pressures of up to 100 GPa.

3.6.2. Cryostats for single-crystal XAS. XAS measurements on single crystals is challenging due to the presence of Bragg peaks in the spectrum when scanning the energy. The spectral quality in this case is greatly improved by mounting the sample on a rotating sample holder to smooth out the distortions due to Bragg peaks. To perform this kind of measurement at cryogenic temperature, we have developed a small turbine driven by a nitrogen-gas flow supplied by a cold gas generator

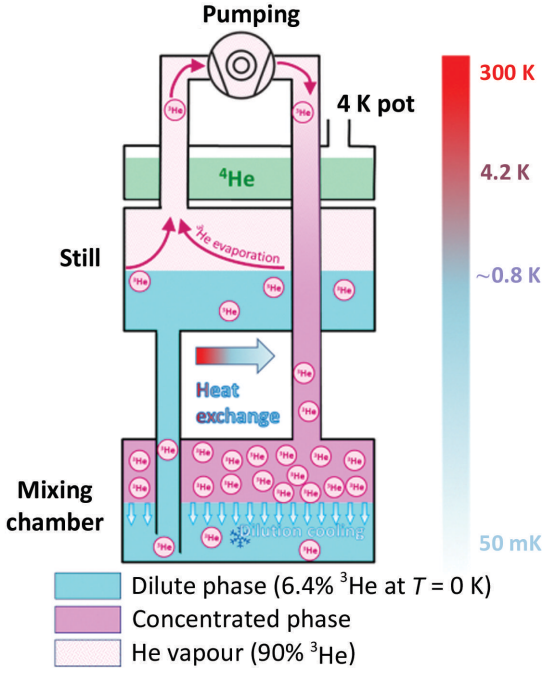

Figure 4
Principle of the ^{3}He–^{4}He dilution refrigerator.

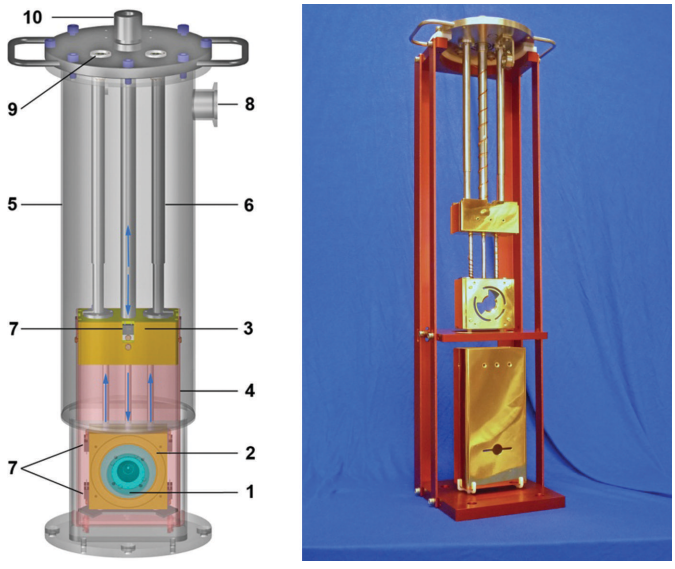

Figure 5
Cryostat developed for XAS/XMCD under high pressure. (1) High-pressure cell, (2) main heat exchanger, (3) secondary heat exchanger, (4) thermal screen, (5) vacuum chamber, (6) telescopic supports, (7) heaters, (8) vacuum port, (9) connectors and (10) L-He fitting.

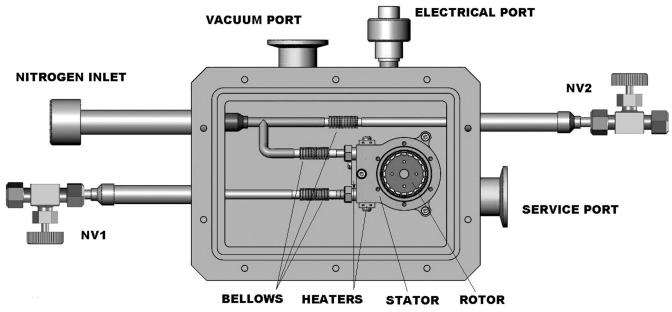

Figure 6
Cryoturbine for single-crystal XAS measurements

that rotates the sample at a given frequency (Fig. 6). The sample is cooled by the flow of nitrogen and can reach frequencies up to 100 Hz with good mechanical stability (Pasternak *et al.*, 2007).

3.6.3. Cryostats for submicrometre XAS applications. Small samples or submicrometre beams impose mechanical stability conditions that require special procedures in the design and construction of the cryostat, such as structural stabilization by raw material annealing or the use of low expansion coefficient materials (INVAR). It also requires the temperature gradients in sensitive parts of the cryostat to be fixed using several temperature-control loops. This kind of technology allowed the first heterogeneous quantum structures at the submicrometre scale to be observed (Martínez-Criado *et al.*, 2007). Currently, the stability level is better than 100 nm at low temperature (8 K) measured with a beam of 50 × 50 nm (Steinmann *et al.*, 2020).

4. Conclusion

It is clear that cryogenic techniques play a key role in the investigation of matter by XAS, whether it be for sample preservation, Debye–Waller minimization or low-temperature phase studies. Cryogenic technologies cover a wide domain and there is no single cryogenic solution for all kinds of XAS experimental techniques. The choice of a cryostat must take into account the specific scientific goal of the beamline and the nature of the sample. In particular, the sample-thermalization method is crucial for data reliability, and the effects of the X-ray beam on the sample temperature must be carefully evaluated. Often an XAS beamline needs to be equipped with multiple cryogenic devices to cover a large variety of scientific cases.

Owing to the scarcity of helium, laboratories should have facilities to capture and recover helium as it comes out of the cryostat. In the future, the use of cryo-free systems will certainly spread even more rapidly if their main drawback (low cooling power) can be improved.

Acknowledgements

We are extremely grateful to Hugo Vitoux, Sebastien Pasternak and Florian Perrin (ESRF) for technical support during the construction and commissioning of cryostats.

References

Abd el All, N., Dalba, G., Diop, D., Fornasini, P., Grisenti, R., Mathon, O., Rocca, F., Thiodjio Sendja, B. & Vaccari, M. (2012). *J. Phys. Condens. Matter*, **24**, 115403.
Beeck, T., Baev, I., Gieschen, S., Meyer, H., Meyer, S., Palutke, S., Feulner, P., Uhlig, K., Martins, M. & Wurth, W. (2016). *Rev. Sci. Instrum.* **87**, 045116.
Betts, D. S. (1989). *An Introduction to Millikelvin Technology*. Cambridge University Press.
Bridges, F., Keiber, T., Juhas, P., Billinge, S. J. L., Sutton, L., Wilde, J. & Kowach, G. R. (2014). *Phys. Rev. Lett.* **112**, 045505.
Cao, D., Bridges, F., Kowach, G. R. & Ramirez, A. P. (2003). *Phys. Rev. B*, **68**, 014303.
Caramazza, S., Marini, C., Simonelli, L., Dore, P. & Postorino, P. (2016). *J. Phys. Condens. Matter*, **28**, 325401.
Chantler, C. T. (2021). *Int. Tables Crystallogr. I*, https://doi.org/10.1107/S1574870721003785.
Conte, R. R. (1970). *Eléments de Cryogénie*. Paris: Masson.
Croft, M., Caliebe, W., Woo, H., Tyson, T. A., Sills, D., Hor, Y. S., Cheong, S.-W., Kiryukhin, V. & Oh, S.-J. (2003). *Phys. Rev. B*, **67**, 201102.
Dalba, G., Fornasini, P., Kuzmin, A., Purans, J. & Rocca, F. (1995). *J. Phys. Condens. Matter*, **7**, 1199–1213.
Fornasini, P. & Grisenti, R. (2014). *J. Chem. Phys.* **141**, 164503.
Fornasini, P. & Grisenti, R. (2015). *J. Synchrotron Rad.* **22**, 1242–1257.
Gatteschi, D. & Sessoli, R. (2003). *Angew. Chem. Int. Ed.* **42**, 268–297.
George, G. N., Pickering, I. J., Pushie, M. J., Nienaber, K., Hackett, M. J., Ascone, I., Hedman, B., Hodgson, K. O., Aitken, J. B., Levina, A., Glover, C. & Lay, P. A. (2012). *J. Synchrotron Rad.* **19**, 875–886.
Joseph, B., Iadecola, A., Puri, A., Simonelli, L., Mizuguchi, Y., Takano, Y. & Saini, L. (2010). *Phys. Rev. B*, **82**, 020502.
Kappler, J.-P., Otero, E., Li, W., Joly, L., Schmerber, G., Muller, B., Scheurer, F., Leduc, F., Gobaut, B., Poggini, L., Serrano, G., Choueikani, F., Lhotel, E., Cornia, A., Sessoli, R., Mannini, M., Arrio, M.-A., Sainctavit, P. & Ohresser, P. (2018). *J. Synchrotron Rad.* **25**, 1727–1735.
Kummer, K., Fondacaro, A., Jimenez, E., Velez-Fort, E., Amorese, A., Aspbury, M., Yakhou-Harris, F., van der Linden, P. & Brookes, N. B. (2016). *J. Synchrotron Rad.* **23**, 464–473.
Latimer, M. J., Ito, K., McPhillips, S. E. & Hedman, B. (2005). *J. Synchrotron Rad.* **12**, 23–27.
Letard, I., Sainctavit, P., dit Moulin, C. C., Kappler, J.-P., Ghigna, P., Gatteschi, D. & Doddi, B. (2007). *J. Appl. Phys.* **101**, 113920.
Linden, P. van der, Vitoux, H., Steinmann, R., Vallone, B. & Ardiccioni, C. (2013). *J. Phys. Conf. Ser.* **425**, 012015.
Lounasmaa, O. V. (1974). *Experimental Principles and Methods Below 1 K*. London: Academic Press.
MacDonald, M. A., Chevrier, D. M., Zhang, P., Qian, H. & Jin, R. (2011). *J. Phys. Chem. C*, **115**, 15282–15287.
Manceau, A., Marcus, M. A. & Tamura, N. (2002). *Rev. Mineral. Geochem.* **49**, 341–428.
Mannini, M., Pineider, F., Sainctavit, P., Danieli, C., Otero, E., Sciancalepore, C., Talarico, A. M., Arrio, M.-A., Cornia, A., Gatteschi, D. & Sessoli, R. (2009). *Nat. Mater.* **8**, 194–197.
Martínez-Criado, G., Steinmann, R., Alén, B., Labrador, A., Fuster, D., Ripalda, J. M., Homs, A., Labouré, S. & Susini, J. (2007). *Rev. Sci. Instrum.* **78**, 025106.
McFarlane Holman, K. L., Latimer, M. J. & Yachandra, M. J. (2004). *Rev. Sci. Instrum.* **75**, 2056–2060.
Mesu, J. G., Beale, A. M., de Groot, M. F. & Weckhuysen, B. M. (2006). *J. Phys. Chem. B*, **110**, 17671–17677.
Mizumaki, M., Tsutsui, S., Uruga, T., Tanida, H., Kikuchi, D., Sugawara, H. & Sato, H. (2011). *J. Phys. Soc. Jpn*, **80**, 074603.
Okabayashi, J., Ueno, S., Wakisaka, Y. & Kitazawa, T. (2015). *Inorg. Chim. Acta*, **426**, 142–145.

Okane, T., Takeda, Y., Yamagami, H., Fujimori, A., Matsumoto, Y., Kimura, N., Komatsubara, T. & Aoki, H. (2012). *Phys. Rev. B*, **86**, 125138.
Palmer, A., Silevitch, D. M., Feng, Y. J., Wang, Y. S., Jaramillo, R., Banerjee, A., Ren, Y. & Rosenbaum, T. F. (2015). *Rev. Sci. Instrum.* **86**, 093901.
Pasternak, S., Perrin, F., Ciatto, G., Palancher, H. & Steinmann, R. (2007). *Rev. Sci. Instrum.* **78**, 075110.
Pobell, F. (2007). *Matter and Methods at Low Temperatures*. Berlin, Heidelberg: Springer-Verlag.
Richardson, R. C. & Smith, E. N. (1988). *Experimental Techniques in Condensed Matter Physics at Low Temperatures*. Boca Raton: CRC Press.
Schooneveld, M. M. van & DeBeer, S. (2015). *J. Electron Spectrosc. Relat. Phenom.* **198**, 31–56.
Sevillano, E., Meuth, H. & Rehr, J. J. (1979). *Phys. Rev. B*, **20**, 4908–4911.
Steinmann, R. G., Martinez-Criado, G., Salomon, D., Vitoux, H., Tucoulou, R., Villanova, J., Laboure, S., Eymery, J. & Segura-Ruiz, J. (2020). *J. Synchrotron Rad.* **27**, 1074–1079.
Strohm, C., van der Linden, P., Mathon, O. & Pascarelli, S. (2019). *Phys. Rev. Lett.* **122**, 127204.
Subías, G., García, J. & Blasco, J. (2005). *Phys. Rev. B*, **71**, 155103.
Timoshenko, J., Anspoks, A., Kalinko, A. & Kuzmin, A. (2014). *Acta Mater.* **79**, 194–202.
Wallander, H. & Wallentin, J. (2017). *J. Synchrotron Rad.* **24**, 925–933.
Wang, P., McKenna, B. A., Menzies, N. W., Li, C., Glover, C. J., Zhao, F.-J. & Kopittke, P. M. (2019). *J. Synchrotron Rad.* **26**, 1272–1279.
Yamazoe, S., Takano, S., Kurashige, W., Yokoyama, T., Nitta, K., Negishi, Y. & Tsukuda, T. (2016). *Nat. Commun.* **7**, 10414.